Journal of Molecular Catalysis A: Chemical 298 (2009) 115–124

Contents lists available at ScienceDirect

Journal of Molecular Catalysis A: Chemical

journal homepage: www.elsevier.com/locate/molcata

Low temperature carbon monoxide oxidation over gold nanoparticles supported on sodium titanate nanotubes

Jui-Ying Tsai [a], Jiunn-Hsing Chao [b], Chiu-Hsun Lin [a,*]

[a] Department of Chemistry, National Changhua University of Education, Changhua 500, ROC, Taiwan
[b] Nuclear Science and Technology Development Center, National Tsing Hua University, Hsinchu 300, ROC, Taiwan

ARTICLE INFO

Article history:
Received 21 April 2008
Received in revised form
19 September 2008
Accepted 4 October 2008
Available online 18 October 2008

Keywords:
Gold
Sodium titanate nanotube
CO oxidation
Ion exchange

ABSTRACT

Small gold particles having sizes of 1.0–2.0 nm were deposited on the surface of the sodium trititanate ($Na_2Ti_3O_7$) nanotube by the ion exchange method. This nanotube-supported gold catalyst was able to oxidize CO at the sub-ambient temperature. In a pulse reactor, the gold catalyst could achieve a $T_{50\%}$ of 218 K using 1.0 vol.% CO/He gas pulses (0.34 μmol CO/pulse). In the Au loadings of 0.39–2.53 wt.%, the activity of the gold catalyst increased with the gold loading. Calcination of nanotube support at higher than 383 K prior to the gold deposition produced a catalyst with a lower activity. Regarding the effect of calcining the gold particles on the activity (with NaTNT support calcined at 673 K), the catalyst with gold particles heated at 383 K only exhibited the best CO oxidation activity. XPS indicated that there are three gold species with different oxidation state, Au^0, Au^{+1} and $Au^{\delta-}$, in the calcined gold catalysts. As calcination temperature increased, the Au^0 concentration increased at the consumption of Au^{+1} species, while the $Au^{\delta-}$ concentration remained relatively constant. This fact strongly suggested that Au^{+1} species must play an important role in the activity in the sub-ambient temperature region.

1. Introduction

Gold is normally regarded as an inert noble metal for catalytic purposes. Nevertheless, in the late 1980s Haruta reported that a supported gold catalyst was able to catalyze the oxidation of CO to CO_2 even at 203 K [1,2]. Since then, there has been a surge in the number of papers published in this field to investigate the mysterious catalytic effect of such gold catalyst. Intensive research efforts have been concentrating on using various preparation techniques to prepare supported gold particles such as co-precipitation [3], co-sputtering [4], chemical vapor deposition [5], impregnation [6], grafting [7], photodeposition [8], physical mixing [9], low-energy cluster beam deposition [10], adsorption of gold colloids on metal oxides [11], and ion exchange [12]. Even though small gold particles are active for CO oxidation, the oxide support definitely plays a role. It had been demonstrated that the support affected the dispersion [13] and shape of the gold particles [14]. In addition, the presence of defect sites on the oxide surface was known to provide sites for nucleation and growth of metal particles [15]. Both non-reducible (e.g., γ-Al_2O_3 [16], MgO [17], SiO_2 [18]) and reducible metal oxides (e.g., Fe_2O_3 [19], CeO_2 [20] and TiO_2 [6]) had been utilized as support materials to prepare active supported gold catalysts.

Furthermore, it has been widely recognized that only the preparation method able to produce gold particles with a size smaller than 5 nm on oxide supports can lead to a good performance catalyst [2,6,21]. There is also a consensus in the literature that the choice of support affects the reaction pathway of the supported gold catalyst. For example, the mode of supplying O_2 to the active center in the gold catalyst is different over reducible and non-reducible oxides [2,22]. The effects imposed by the preparation method and the support might also interact with each other, adding more complexity to the research. For instance, using impregnation method with $HAuCl_4$ to prepare Au/TiO_2 resulted in a large Au particle (>20 nm) and less active catalyst after thermal treatment to form the metallic gold particles [23]. The formation of large gold particles was attributed to both the weak interaction between the $HAuCl_4$ and the support and the presence of chlorides in the catalyst to promote the sintering of the gold particles during the thermal treatment.

Recently, Kasuga reported the preparation of a mesoporous sodium titanate nanotube (NaTNT) using a hydrothermal method, in which TiO_2 powder was treated in a concentrated NaOH solution at the elevated temperatures [24,25]. Due to the high sensitivity of the phase composition to the preparation condition, a number of crystal structures had been proposed for this titanate nanotube such as dititanate ($Na_2Ti_2O_4(OH)_2$) [26], trititanate ($Na_2Ti_3O_7$) [27], tetratitante ($Na_2Ti_4O_8(OH)_2$) [28], and lepidocrocite ($H_xTi_{2-x/4}\square_{x/4}O_4H_2O$ where $x = 0.7$ □ = vacancy) [29].

* Corresponding author. Tel.: +886 4 7232105x3541; fax: +886 4 7292361.
E-mail address: chlin@cc.ncue.edu.tw (C.-H. Lin).

1381-1169/$ – see front matter © 2008 Elsevier B.V. All rights reserved.
doi:10.1016/j.molcata.2008.10.019

It is known that alkali metal titanates with a layered structure are good ion exchangers [30,31]. Ion exchange itself has been a useful technique to prepare highly dispersed precious metal catalysts in heterogeneous catalysis [12,32,33]. Nevertheless, there are very few reports to explore the ion exchange ability of the newly synthesized NaTNT [33,34]. In this manuscript, we have shown that small gold particles having sizes of 1.0–2.0 nm could be prepared on the NaTNT surface by ion exchange with $AuCl_3$, and this titanate nanotube-supported gold catalyst (AuNaTNT) displayed an exceptional activity in the oxidation of CO to CO_2 at the sub-ambient temperature. This AuNaTNT catalyst contained three gold species with different oxidation states (Au^0, Au^{+1} and $Au^{\delta-}$) and the presence of Au^{+1} species is crucial for the catalytic activity in the sub-ambient temperature region.

2. Experimental

2.1. Preparation of NaTNT and AuNaTNT

To prepare sodium titanate nanotube, 1.5 g of anatase TiO_2 powder was mixed with 600 ml of 10 M NaOH in a 1.0 L perfluoroalkoxy container and the mixture was kept at 383 K for seven days with vigorous stirring. The resulting slurry was filtered and washed a few times with deionized water. The washed product was filtered to yield a cake, which was dried at 383 K overnight to yield NaTNT. The NaTNT was further calcined at between 473 K and 673 K in ambient air for 3 h using a heating rate of 1 K min^{-1}.

Different weight percentage of gold was introduced into NaTNT by ion exchange with $AuCl_3$ (99.9%, Aldrich). Appropriate amount of the $AuCl_3$ was mixed with 250 mL of deionized water, into which 0.50 g of NaTNT was added and stirred for 24 h at room temperature. The pH of the suspension solution was then adjusted with 0.10 M NaOH to 10 to lower the zeta potential of NaTNT in order to eliminate the adsorption of chloride ions. The resulting solution was filtered, and the obtained solid was washed with deionized water and dried at 383 K for 1 h to yield a pale yellow powder. Generally speaking, about 50–85% of the calculated amount of gold could be loaded into the titanate nanotube with the above preparation procedure. To examine the effect of calcination temperature on the gold particles, the pale yellow powder was calcined again as previously between 473 K and 673 K, yielding AuNaTNT with a purple color. It should be mentioned that the color of AuNaTNT catalysts became darker purple after CO oxidation reaction. The catalyst was labeled as AuT1-ST2-wt.% of Au, where AuT1 and ST2 denoted the calcination temperatures of gold precursor and of NaTNT support, respectively. Literature had reported that the gold complex used to prepare the supported gold catalyst would be decomposed by light and that the size of the gold metal particle would increase when exposed to light or ambient air (due to its moisture content) during storage [35]. Therefore, all the experimental procedures including preparation, characterization and catalytic activity measurements should be conducted in the absence of light as much as possible, and the prepared AuNaTNT catalysts were stored in brown bottles under dry N_2 atmosphere and placed the dark.

2.2. Characterization of catalysts

The BET surface areas of the catalysts were measured with Micromeritics ASAP 2010 using N_2 as the adsorbate, and their pore size distributions were determined by the BJH method. X-ray powder diffraction patterns of the calcined gold catalysts were obtained using a Shimadzu Lab-X XRD-6000 spectrometer with Cu Kα irradiation (λ = 1.5418 Å) at 30 kV and 30 mA. A JEOL JSM-6700F field-emission scanning electron microscope (FE-SEM) operated at 15 kV was employed to observe the morphology of the nanotubes. The FE-SEM samples were prepared by adding a drop of aqueous solution that contained the sample onto a 4 mm × 5 mm silicon wafer followed by drying at 383 K. The sample-loaded wafer was coated with a thin layer of gold by sputtering before the FE-SEM experiments. A Phillips Tecnai G2 F20 transmission electron microscope at an accelerating voltage of 200 kV was adopted to observe the fine structure of AuNaTNT. A copper grid that was coated with a holey carbon film was used to prepare the samples for HRTEM observation. The powder sample was dispersed in ethanol and the resulting suspension was treated in an ultrasonic bath for 1 h. The copper grid was then dipped into the ethanol for a few seconds to fix the sample onto the copper grid, which was dried in the atmosphere overnight before TEM experiments. The determination of Au particle size distribution using HRTEM was measured over 100 particles. XPS spectra were obtained with PHI Quantera SXM X-ray photoelectron spectrometer. A charge-compensating electron gun was used during recording the XPS spectra to avoid catalyst charging. The vacuum inside the analysis chamber was better than 3×10^{-8} torr.

The diffuse reflectance infrared Fourier transformation (DRIFT) spectra of NaTNT were recorded by using an Equinox 55 spectrometer (Bruker) equipped with a diffuse reflectance accessory (Praying Mantis, Harrick) and a high temperature cell with KBr windows (HVC, Harrick). 50 mg of catalyst powder was loaded in the high temperature cell and evacuated ($<6 \times 10^{-5}$ torr) at 383 K for 1 h prior to the spectra recording. DRIFT spectra were recorded using a resolution of 4 cm^{-1} and 128 scans. The gold contents in these AuNaTNT catalysts were determined by neutron irradiation. Four samples of NaTNT spiked with known amount of Au were used as calibration standards. The standards and samples were pressed into tablets and irradiated with a 15 MV X-ray from a medical accelerator (Primus, Simens) for a period of time, and the emitted neutrons were subsequently measured by photodiode detector (Model 1135, Sun Nuclear Corporation). The medical accelerator, which is part of the facility of Changhua Christian hospital, is routinely used for cancer therapy.

2.3. Measurement of the catalytic activity in a pulse flow reactor

The measurement of the catalytic reactivity was performed in an AutoChem 2910 analyzer (Micromeritics) equipped with a liquid N_2 cryo-cooler to control the sub-ambient temperature. The AutoChem 2910 was operated in a pulse reactor mode, and its diagram is depicted in Scheme 1. In a typical experiment, 50 mg of catalyst was packed inside the U-shape quartz reactor held by a quartz wool plug, and was dried at 393 K in 10 vol.% O_2/He at a flow rate of 30 mL min^{-1} for 1 h. After pretreatment, 10 vol.% O_2/He continuously flowed through the catalyst bed, while the temperature of the oven was controlled between 183 K and 393 K at an interval of 5 K. At each selected temperature the reactor was operated isothermally, and two pulses of gaseous mixture containing 1 vol.% CO in He (0.34 μmol CO/pulse) were injected into the O_2/He gas stream through the sampling loop to obtain the CO conversions. The product mixture were analysed by an on-line quadrupole mass spectrometer (Prolab, Thermo Onix), and the average value of the two CO conversions was adopted as the conversion of the temperature. Such pulse experiment was repeated three times for each catalyst so that a total of 258 data points were collected in a single activity test. The CO conversion plots presented in the manuscript were those obtained from the third run of the pulse experiment. The CO conversions were calculated based on the amount of CO_2 produced according to the following equation,

$$\text{CO conversion}\,(\%) = \left(\frac{A_{CO_2}}{A_{CO_2,100\%}}\right) \times 100$$

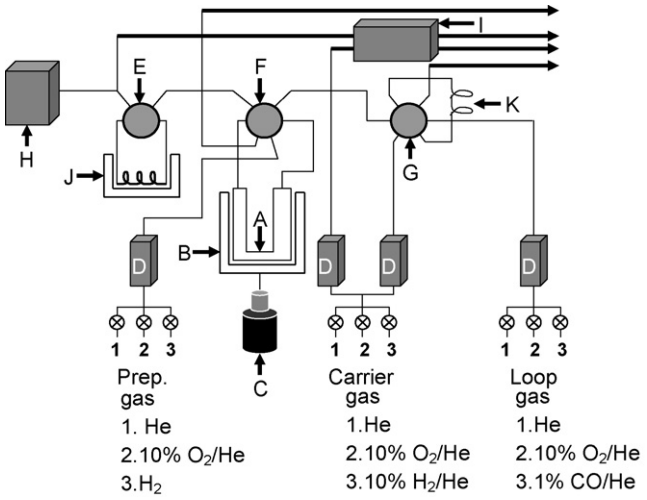

Scheme 1. The reactor diagram of Autochem 2910 analyzer, (A) U-shape quartz reactor; (B) oven; (C) liquid N_2 cryo-cooler; (D) mass flow controller; (E) two-way valve; (F) two-way valve; (G) two-way valve; (H) quadrupole mass spectrometer; (I) TCD; (J) cold trap; (K) injection loop.

where A_{CO_2}: peak area of CO_2 ($m/e = 44$), and $A_{CO_2,100\%}$: peak area of CO_2 corresponding to 100% conversion of CO ($m/e = 28$).

3. Results and discussion

3.1. Characterization of morphology, microstructure and Au particle size of AuNaTNT by electron microscopy

Fig. 1a displays the FE-SEM micrograph of the anatase TiO_2 powder that was used to prepare NaTNT. It indicates that the starting material comprises round particles of sizes 50–250 nm. Fig. 1b is the FE-SEM micrograph of the hydrothermal product after washing in deionized water and drying at 383 K. The micrograph shows that the hydrothermal product consists of many fiber-like materials with diameters of 20–150 nm and lengths of up to a micrometer. The HRTEM micrograph in Fig. 1c reveals that the fiber-like material with a larger diameter is actually comprised of a few smaller hollow tubes with outer diameters of around 10 nm, binding to each other to form a nanotube-bundle. The HRTEM micrograph of a section of the nanotube loaded with two spherical gold nanoparticles is displayed in Fig. 1d. This micrograph indicates that the nanotube has an outer diameter around 9 nm and a hollow inside diameter of 4.5 nm. The inside diameter of the nanotube obtained by HRTEM is close to the pore diameter measured by the low temperature adsorption of the N_2 (see Section 3.2). This micrograph also shows

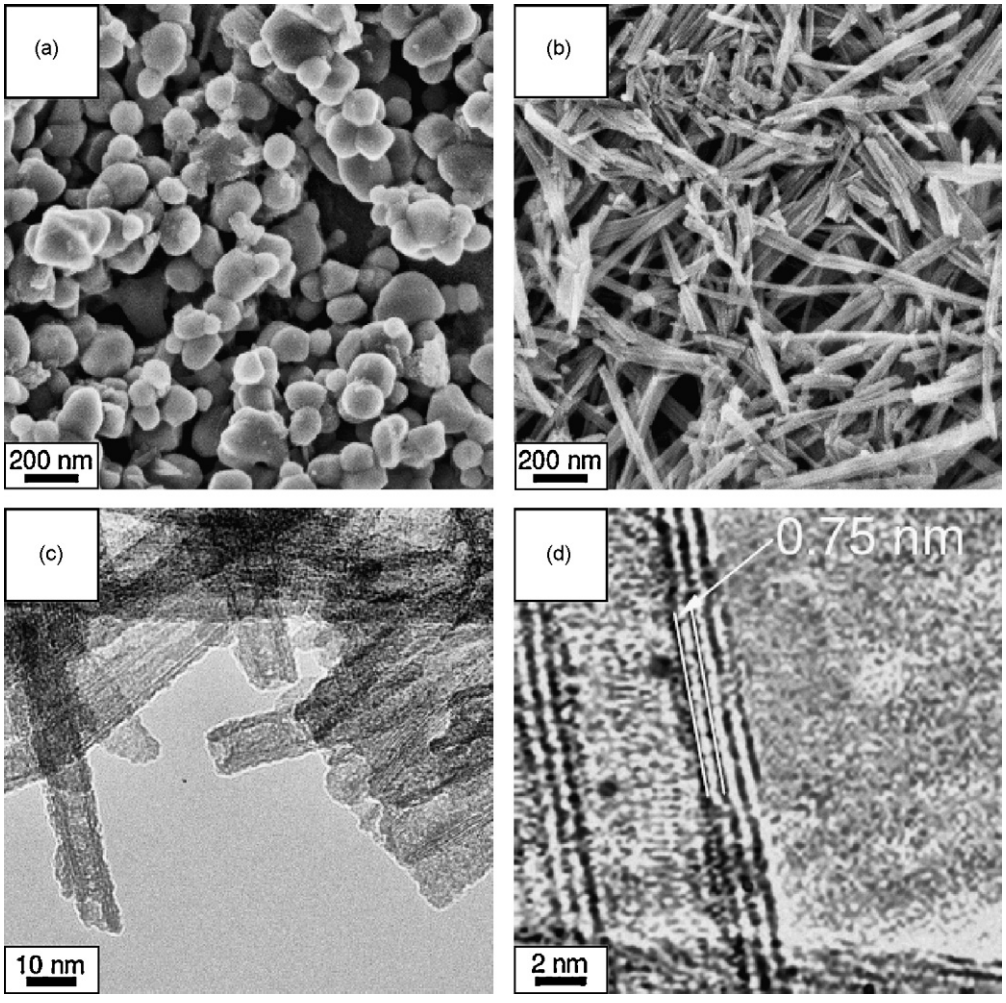

Fig. 1. (a) FE-SEM micrograph of anatase particles, (b) FE-SEM micrograph of NaTNT dried at 383 K, (c) TEM micrograph of NaTNT dried at 383 K, and (d) HRTEM micrograph of AuNaTNT dried at 383 K showing the image of the gold particles and the lattice fringe of NaTNT.

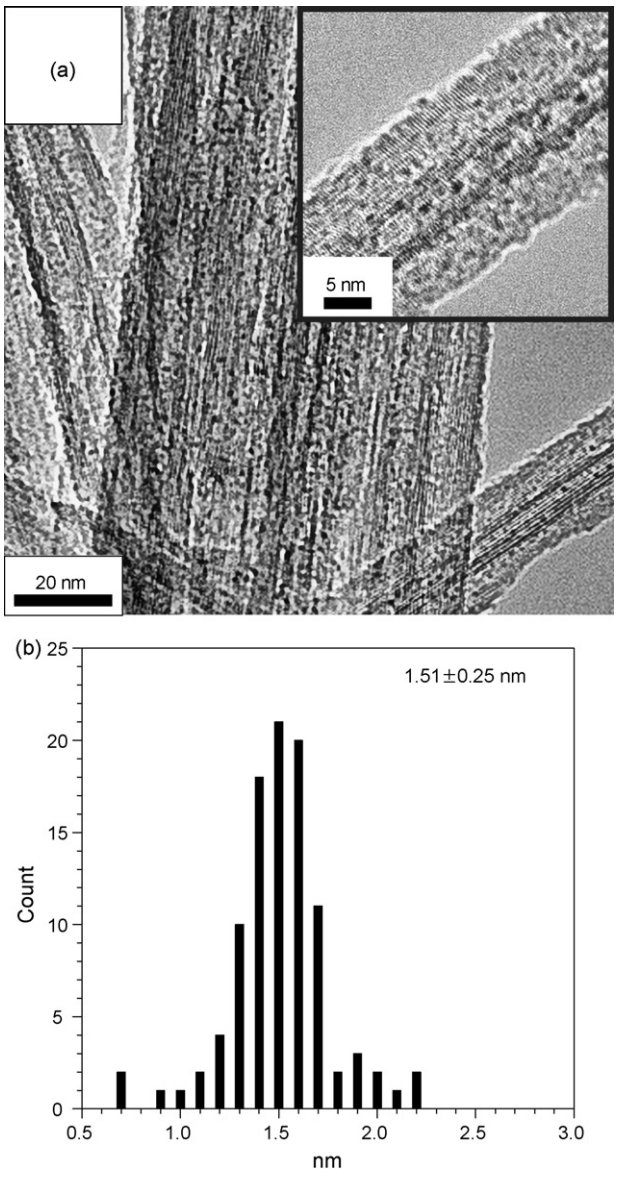

Fig. 2. (a) TEM micrograph of AuNaTNT with 2.53 wt.% of gold loading and dried at 383 K, and the insert is a magnified image of a selected region, and (b) gold particle size distribution of AuNaTNT in (a).

that the nanotube has a lattice fringe of 0.75 nm, whose value is the interplanar distance of (2 0 0) crystal plane of a sodium trititanate ($Na_2Ti_3O_7$) [36].

The gold particle size distribution and the location of gold particles on the titanate nanotube surface are depicted in Fig. 2 for AuNaTNT (Au383-S383-2.53). As can be seen in the micrograph in Fig. 2a, the gold particles are distributed quite homogeneously on the NaTNT surface, showing no preference of anchoring sites. The gold particle size deposited by the ion exchange method on NaTNT is rather small and the average gold particle size observed in HRTEM was about 1.51 ± 0.25 nm (Fig. 2b). Furthermore, the gold particle size distribution is quite narrow, and most of the gold particles have diameters within 1.0 and 2.0 nm. Numerous investigations on low temperature CO oxidation had shown that gold catalysts with a small particle size (<5 nm) were more active on a variety of oxide supports [16,20,37]. The origin of the exceptional catalytic activity of small gold particles is the presence of undercoordinated atoms, which are sites for binding O_2 and CO [38,39]. Theoretical calculations indicated that the number of undercoordinated atom (step density) increases continuously as the particle size decreases [40]. In addition, these undercoordinated sites have lower adsorption energies for both CO and O atoms (stronger Au–CO and Au–O bonds) [38]. Therefore, it is reasonable to expect that AuNaTNT containing nanosized gold particles should be an active catalyst for low temperature oxidation of CO.

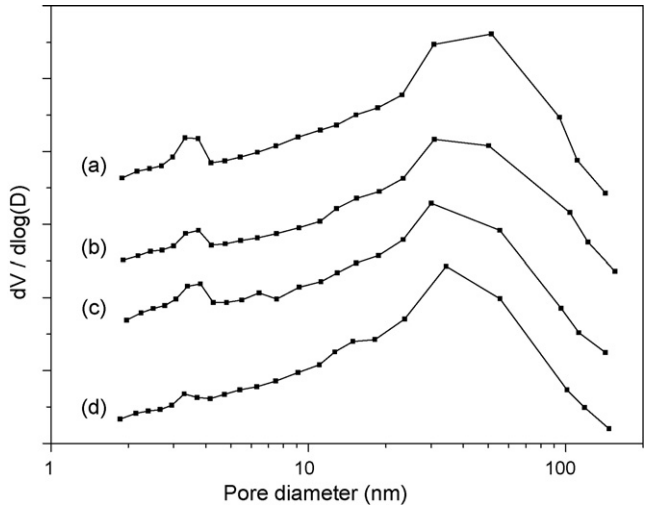

Fig. 3. The pore size distributions of NaTNT calcined at (a) 383 K, (b) 473 K, (c) 573 K, and (d) 673 K.

3.2. Surface area and pore structure characterization of NaTNT and AuNaTNT

Fig. 3 presents the pore size distributions of the NaTNT that were calcined between 383 K and 673 K. The figure reveals a bipolar distribution of pore diameters, whose maximum are located at 3–5 nm and 30–50 nm, respectively. The smaller pores of 3–5 nm corresponds to the inside diameters of the NaTNT, and the larger pores of 40–50 nm are the space between the nanotubes in the nanotube-bundle and that between the nanotube-bundles. As nanotubes and nanotube-bundles are randomly arranged, it is natural that the large pore of NaTNT has a wide distribution of pore size. Furthermore, when these nanotubes were calcined at 673 K, the volume of small pore was shrunk significantly but that of the large pore decreased only slightly. Table 1 summarizes the physical properties of NaTNT and AuNaTNT at various calcination temperatures.

Table 1
The physical properties and $T_{50\%}$ for NaTNT and AuNaTNT calcined at various temperatures.

Catalysts	BET surface area (m^2/g)	Pore volume (cm^3/g)	$T_{50\%}$ (K)
Au383-S383-0.39	141	0.45	246
Au383-S383-0.86	142	0.46	242
Au383-S383-1.39	140	0.46	238
Au383-S383-2.53	141 (144)[a]	0.45 (0.46)	218
Au383-S473-2.50	129 (131)[a]	0.43 (0.43)	232
Au383-S573-2.37	103 (106)[a]	0.42 (0.42)	250
Au383-S673-2.20	81 (83)[a]	0.36 (0.37)	263
Au473-S673-2.20[b]	85	0.34	270
Au573-S673-2.20[b]	82	0.33	284
Au673-S673-2.20[b]	80	0.35	292

[a] The number in the parenthesis is the surface area and total pore volume for the NaTNT support.

[b] These catalysts are prepared by calcining Au383-S673-2.20 between 473 K and 673 K.

The surface area and pore volume of NaTNT that was dried at 383 K were 144 $m^2 g^{-1}$ and 0.46 $cm^3 g^{-1}$, respectively, decreasing to 83 $m^2 g^{-1}$ and 0.37 $cm^3 g^{-1}$ after calcining at 673 K. The decrease in surface area is mainly due to the loss of small pore, and the fact is also consistent with the slight decrease in the total pore volume. Introducing gold particles into NaTNT by ion exchange did not cause any significant change in surface area and pore volume as indicated in Table 1. In the gold loading of 0.39–2.53 wt.% investigated in this paper, the surface areas and pore volumes of AuNaTNT dried at 383 K remained relatively constant at around 140 $m^2 g^{-1}$ and 0.45 $cm^3 g^{-1}$, similar to those of pure NaTNT. Therefore, introducing gold nanoparticles onto NaTNT by ion exchange do not block the pore of NaTNT to any significant extent.

3.3. Characterization of phase composition of NaTNT and AuNaTNT by XRD

Fig. 4 displays the XRD spectra of the hydrothermal products after washing in deionized water and calcining at between 383 K and 673 K for 3 h. The XRD pattern in Fig. 4a is for the as prepared sample dried at 383 K, and it resembles to those of sodium trititanate ($Na_2Ti_3O_7$) reported in the literatures [34,36]. The XRD spectra did not change significantly with the calcination temperature except that the diffraction peak at $2\theta = 9.9^\circ$ shifted slightly to a larger angle at $2\theta = 10.3^\circ$ as the calcination temperature was increased from 383 K to 673 K. The peak at $2\theta = 9.9^\circ$ was due to the reflection of (2 0 0) crystal plane and the shift toward a higher diffraction angle was attributed to the dehydration of the OH group in NaTNT leading to a smaller interlayer distance in the nanotube wall [26]. The identification of crystalline phase of the nanotube by XRD is consistent with the observed lattice fringe of the material in HRTEM experiment (Fig. 1d), confirming that the crystalline phase of the nanotube is a sodium trititanate. Fig. 5 depicts the XRD spectra of AuNaTNT calcined at between 383 K and 673 K. The XRD data show that below 473 K, the Au particles are so small that they are un-detectable by XRD. However, at between 573 K and 673 K the Au particles start to sinter and a broad and weak peak appears at $2\theta = 77.5^\circ$, which corresponds to the reflection of Au (3 1 1) plane. The average particle sizes estimated by Scherrer equation are 2.6 nm and 3.1 nm, respectively (with a significant error, for the peak is too broad and peak width is difficult to obtain). The latter is close to the average particle size observed by TEM in Fig. 12d [37].

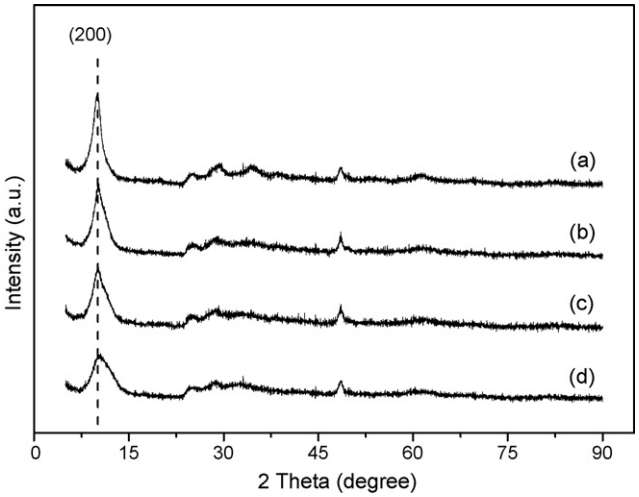

Fig. 4. XRD spectra for NaTNT calcined at (a) 383 K, (b) 473 K, (c) 573 K, and (d) 673 K.

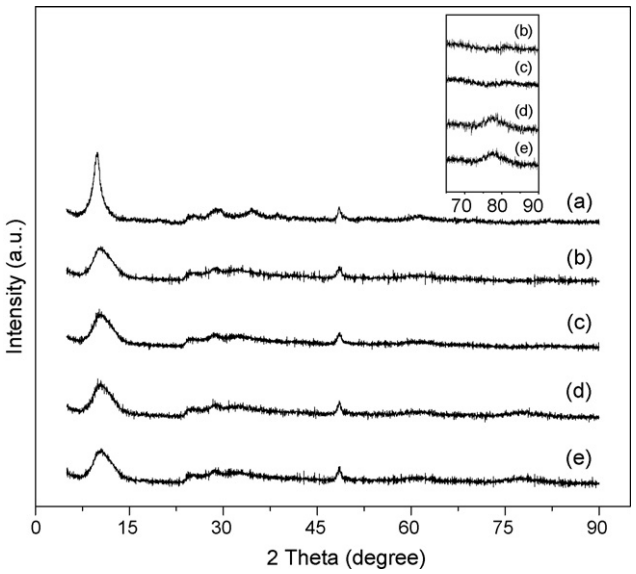

Fig. 5. XRD spectra for (a) AuNaTNT dried at 383 K (Au383-S383-2.53) and for the catalyst (Au383-S673-2.20) calcined for 3 h at (b) 383 K, (c) 473 K, (d) 573 K, and (e) 673 K. Insert includes the expanded peaks at $2\theta = 77.5^\circ$ to estimate the particle sizes in b–e.

3.4. Low temperature oxidation of CO over AuNaTNT catalysts

3.4.1. Catalytic activity in a pulse reactor

Fig. 6 is the CO conversions vs. temperature profiles for an active AuNaTNT catalyst containing 2.53 wt.% Au. As CO conversion obtained over this catalyst has already reached 100% at 228 K, data points collected at higher than 243 K are not plotted in Fig. 6 for clarity. As indicated in Fig. 6, AuNaTNT starts to oxidize CO to CO_2 at a temperature as low as 198 K with a $T_{50\%}$ of 215 K. On the other hand, the conversions vs. temperature profiles of the second and the third run almost overlap and the $T_{50\%}$ lays slightly higher at 218 K. The results indicate that the catalyst has reached a stable activity after the first run. The rationalization of the difference in catalytic activity between the first run and those of the second and the third runs are the following: The gold content in 2.53 wt.% AuNaTNT is 6.42 μmol, and it requires a maximum amount of 9.63 μmol of CO to reduce the gold oxide in AuNaTNT to metallic

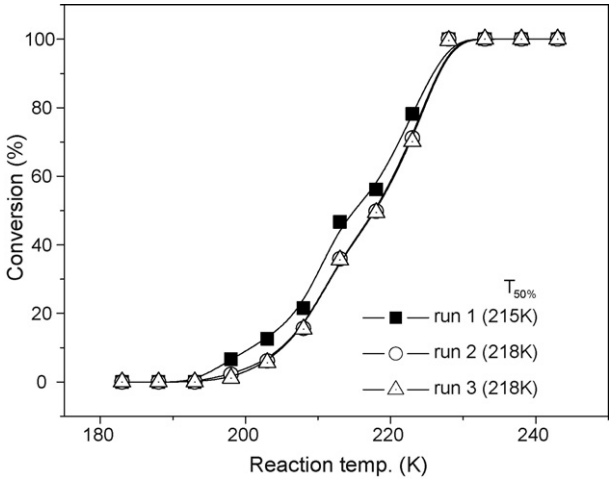

Fig. 6. The CO conversions vs. temperature profile over AuNaTNT with 2.53 wt.% Au and dried at 383 K, showing the CO conversions of the three consecutive runs in a single catalytic activity test.

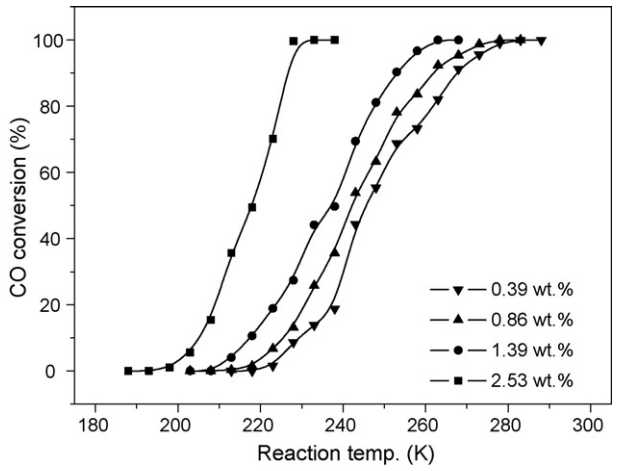

Fig. 7. The CO conversions vs. temperature profile for AuNaTNT with different Au loadings. All the catalysts were dried at 383 K.

gold ($Au_2O_3 + 3CO \rightarrow 2Au + 3CO_2$). Gold oxide such as Au_2O_3 was known to oxidize CO to CO_2 at ambient temperature [9,41]. If there is reduction of gold oxide to proceed, it should be completed in the first run of the catalytic test (at the 29th pulse of CO). The colour of AuNaTNT was purple after drying at 393 K in the flowing O_2, and turned into darker purple after the CO oxidation reaction. Therefore, the CO conversions in the first test run in Fig. 6 might be partly due to stoichiometric reduction of gold oxide into metallic gold, and those in the second and third run should represent the true catalytic activity of AuNaTNT catalyst in the CO oxidation reaction. As a result, we reported only the CO conversions obtained in the third run of the activity test for the rest of the paper. Since the catalyst bed was shielded completely by the furnace of our reactor, the contribution of photocatalytic oxidation of CO over AuNaTNT [42] to the CO conversions measured here should be neligible.

3.4.2. *Effect of Au loading on the catalytic activity*

In the range of Au loading 0.39–2.53 wt.% investigated in this manuscript, all of the AuNaTNT dried at 393 K were active for CO oxidation below the room temperature (Fig. 7). The activities of AuNaTNT catalysts increased with the Au loading: $T_{50\%}$ of catalyst with 2.53 wt.% Au was 218 K, while that of 0.39 wt.% Au was 246 K. The results are the same as observed over Au/TiO_2 with similar gold loading but prepared by DP method [37]. TEM investigations revealed that for AuNaTNT in this Au loading range, an increase in Au loading mainly increased its Au particle density but did not change the Au particle size appreciably. As shown in TEM micrograph in Fig. 8, the Au particle density for AuNaTNT containing 1.39 wt.% Au is 2.2 nm^{-2} (Fig. 8a) with an average Au particle diameter of 1.40 ± 0.43 nm (Fig. 8b), and those for sample containing 0.39 wt.% Au are 1.1 nm^{-2} (Fig. 8c) and 1.42 ± 0.42 nm (Fig. 8d). As this ion exchange method can produce very small Au particles with

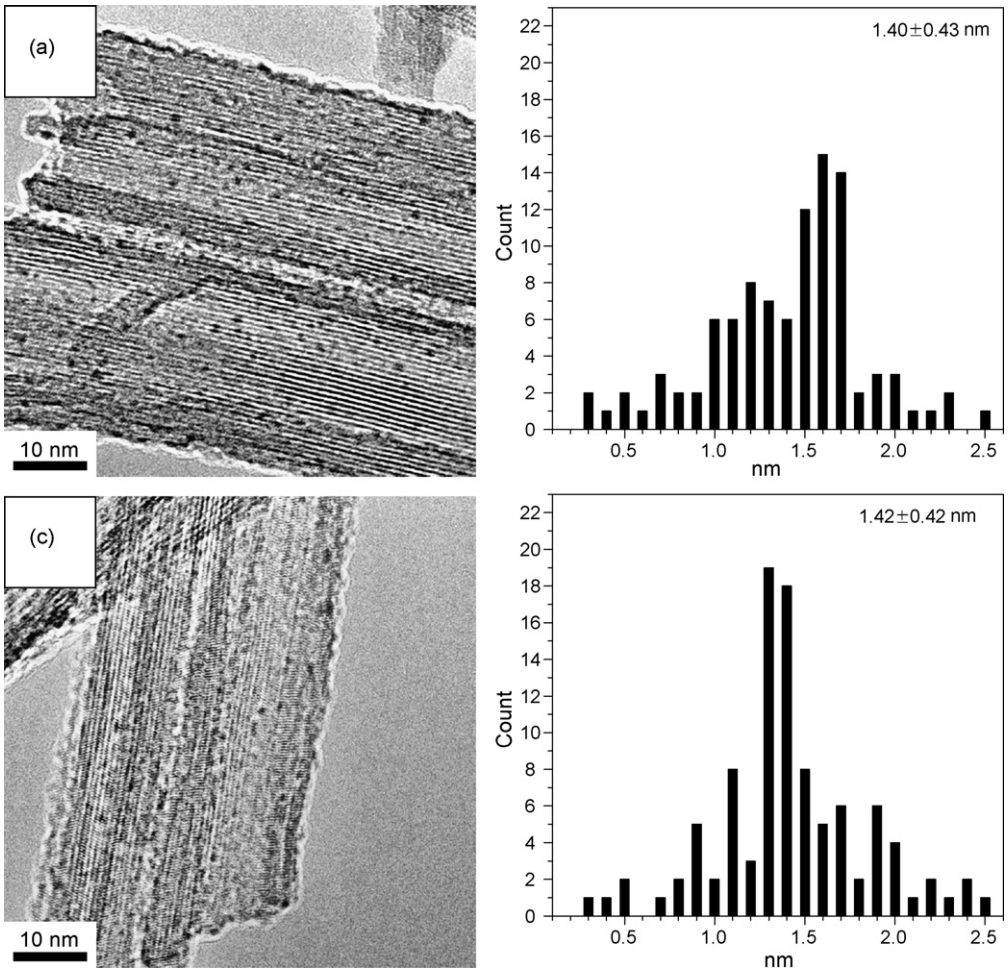

Fig. 8. TEM micrographs of AuNaTNT showing the Au particle size distributions and particle densities for two different Au loadings (a) for 1.39 wt.% AuNaTNT, (b) Au particle size distribution in (a), (c) for 0.39 wt.% AuNaTNT, and (d) Au particle size distribution in (c). These two catalysts are dried at 383 K.

highly undercoordinated sites on the NaTNT surface, it is reasonable to expect that AuNaTNT is an active catalyst in the CO oxidation reaction. Furthermore, a higher Au particle density will result in a longer perimeter at the Au particle–NaTNT interface, which facilitates the adsorption of more O_2 molecules and further enhances the catalytic activity (see more detailed discussion in Section 3.4.3 below).

3.4.3. Effect of support calcination temperature on the catalytic activity

The basic role of oxide support is to provide sites for anchoring gold particles in order to increase the Au metal surface area, and in consequence, to produce a lager number of undercoordinated Au atoms. In addition, the support is thought to contribute to the catalytic activity of Au catalyst through the following mechanisms: (a) the support helps to activate the O_2 molecule [22], (b) the defects on the oxide support can stabilize the small gold particles [15,43,44], (c) water or hydroxyl group on the oxide surface may enhance the catalytic activity [45,46]. We had investigated the support effect by calcining the NaTNT support at between 383 K and 673 K prior to the ion exchange of gold. The variation in CO conversions with respect to calcination temperature is displayed in Fig. 9, where $T_{50\%}$ for catalysts varied between 218 K and 263 K. It is clear that AuNaTNT with support dried only at 383 K was the most active catalyst. Calcining NaTNT at a higher temperature reduced the interlayer distance of (2 0 0) plane of NaTNT, but did not change its the phase composition, as suggested by XRD results depicted in Section 3.3. Calcination did result in the loss of the surface area and pore volume of NaTNT support (see Table 1), which might lead to a smaller Au loading in AuNaTNT and a lower activity. The Au loading, however, decreased only slightly from 2.53% for NaTNT dried at 393 K to 2.20% for that calcined at 673 K.

On the other hand, calcination of NaTNT lowered its moisture content, which was clearly demonstrated in the DRIFT spectra Fig. 10. As can be seen from the IR spectra in Fig. 10, the peaks at 1630 cm^{-1} and 3400 cm^{-1} are the deformation and stretching vibrations of adsorbed water, respectively. In addition, there are a broad peak at 3266 cm^{-1} and two other smaller but sharper peaks at 3658 cm^{-1} and 3731 cm^{-1}, which were attributed to hydrogen-bonded and isolated surface hydroxyl groups on NaTNT, respectively. The peak intensities of the adsorbed water and hydrogen-bonded hydroxyl groups decreased (but did not completely vanish) as the calcination temperature of NaTNT was increased from 383 K to 673 K. Haruta had investigated the effect

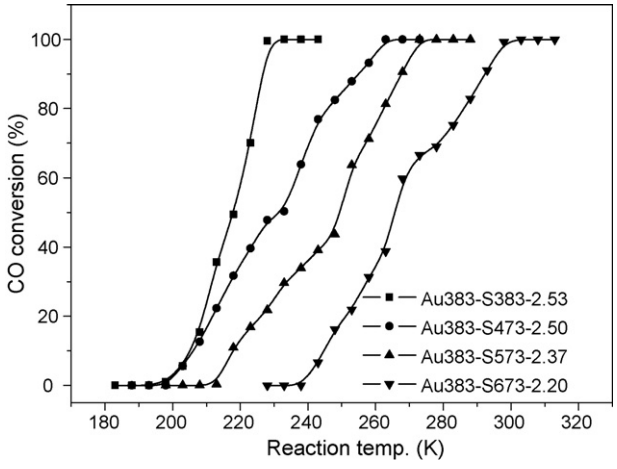

Fig. 9. The variation of CO conversions of AuNaTNT with the calcination temperature of NaTNT support.

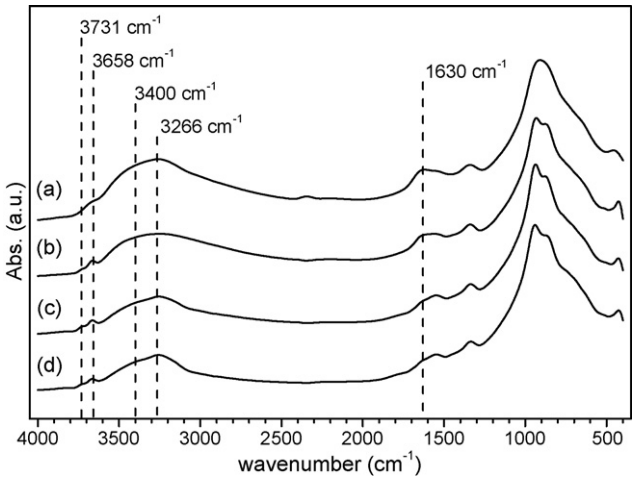

Fig. 10. DRIFT spectra of NaTNT calcined at (a) 383 K, (b) 473 K, (c) 573 K, and (d) 673 K.

of moisture on the activity of Au/TiO_2, and concluded that the low temperature CO oxidation over gold catalyst involves water-derived species on the catalyst surface [45,47]. Furthermore, a recent theoretical work focused on this aspect with several important conclusions [48]: (a) water could dissociate into hydroxyl group at oxygen vacancies of TiO_2 (1 1 0) surface, (b) these hydroxyl species stabilized O_2 adsorption, and (c) O_2 could diffuse along the channel of five-coordinated Ti atoms on TiO_2(1 1 0) to the Au/TiO_2 interface. It is possible that NaTNT without high temperature calcination, having a higher number of OH group, was able to enhance the adsorption of O_2 molecules, and increased the activity of AuNaTNT.

In addition, Wang and Hammer, also through their theoretical calculation results, predicted a strong adhesion of the gold clusters to TiO_2 (1 1 0) surface containing OH groups. The adsorbed clusters became cationic as Au–O bonds formed between gold atoms in the cluster and oxygen atoms of the support [49]. Our results on the calcined NaTNT support are consistent with the above theoretical predictions: (a) AuNaTNT with support calcined at a lower temperature could accommodate a higher Au loading, (b) the presence of higher concentration of cationic Au species in the low temperature-calcined AuNaTNT was confirmed by the XPS results (described in Section 3.4.4 below).

It seems that the existence of OH groups or physically adsorbed water in AuNaTNT is beneficial to its catalytic activity of CO oxidation by increasing the gold loading and creating cationic Au active sites as well as increasing the O_2 supply to the active sites.

3.4.4. Effect of calcination temperature of Au particles on the catalytic activity

Fig. 11 depicts the change in CO conversions for AuNaTNT calcined at between 383 K and 673 K in the ambient air. The NaTNT support used to prepare these AuNaTNT catalysts were calcined at 673 K before Au ion exchange to avoid the support calcination effect. Fig. 11 indicates that $T_{50\%}$ of AuNaTNT increases (becomes less active) as the calcination temperature of Au is increased: the $T_{50\%}$ for AuNaTNT dried at 393 K is 263 K and that calcined at 673 K is 292 K. The activity of AuNaTNT was reduced partly because the gold particle grew larger in size when the calcination temperature was increased in oxidizing or reducing environments [35]. The increase in Au particle size with calcination temperature of AuNaTNT was indeed observed in TEM micrographs in Figs. 2b and 12. The average Au particle sizes for AuNaTNT calcined at 383 K, 473 K and 673 K were 1.51 ± 0.25 nm, 1.82 ± 0.33 nm and 3.37 ± 0.85 nm,

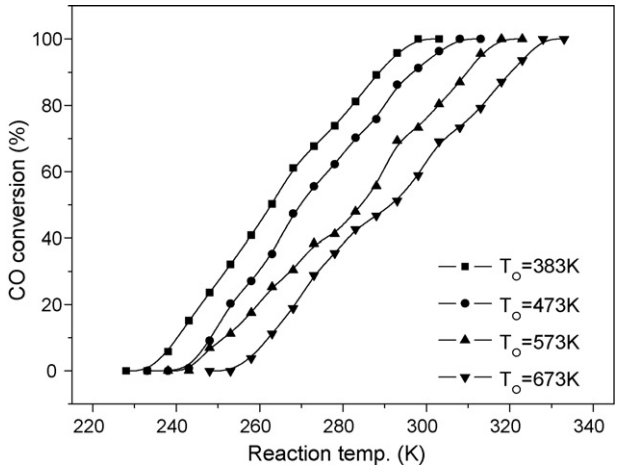

Fig. 11. The variation of CO conversions with gold calcination temperature (T_O). The data in this figure were obtained by calcining the sample Au383-S673-2.20 between 383 K and 673 K.

respectively. Binding between gold particle and NaTNT should be rather strong so that calcination of AuNaTNT at 673 K did not produce Au particles with size greater than 6 nm (Fig. 12d). This might be the reason why even AuNaTNT calcined at 673 K still possessed the capability to oxidize CO at sub-ambient temperatures.

However, the results in Fig. 11 could not be interpreted by the gold particle size alone. Date et al. measured $T_{50\%}$ of Au/TO_2 (DP method) calcined in air at 473 K ($T_{50\%}$ = 245 K), 573 K ($T_{50\%}$ = 235 K), 673 K ($T_{50\%}$ = 250 K) and 873 K ($T_{50\%}$ = 300 K) [50]. Although the average gold particle size for catalyst calcined at 473 K (2.4 nm) was smaller than that calcined at 573 K (3.5 nm), the latter catalyst had a lower $T_{50\%}$ than the former. Their FT-IR/CO adsorption results indicated that the oxidic gold precursors were not completely decomposed into metallic gold particles at 473 K. Park and Lee investigated effect of pretreatment conditions on gold catalysts supported on different oxide supports (Fe_2O_3, TiO_2 and Al_2O_3) [51]. Their results indicated a decreasing CO oxidation activity with an increasing calcination temperature, similar to our results in Fig. 11. X-ray photoelectron spectroscopy (XPS) and X-ray absorption fine structure (XAFS) results indicated that the phase transformation of gold from $Au(OH)_3$ through Au_2O_3 to metallic gold with increasing calcination temperature over all the supported catalysts, and oxidation states of gold were proven important in CO oxidation. Recently, a MgO-supported Au(III) catalyst, whose oxidation state could be controlled under different CO partial pressure in the reaction mixture, was used to study the relationship between the concentration of positively charged gold (Au^+) or metallic gold (Au^0) and the reaction rate. It was found that the presence of cationic Au^+ species in the gold active sites is crucial to the catalytic activity.

We have used XPS to detect the variation of the gold oxidation state in these calcined AuNaTNT catalysts, and the results are

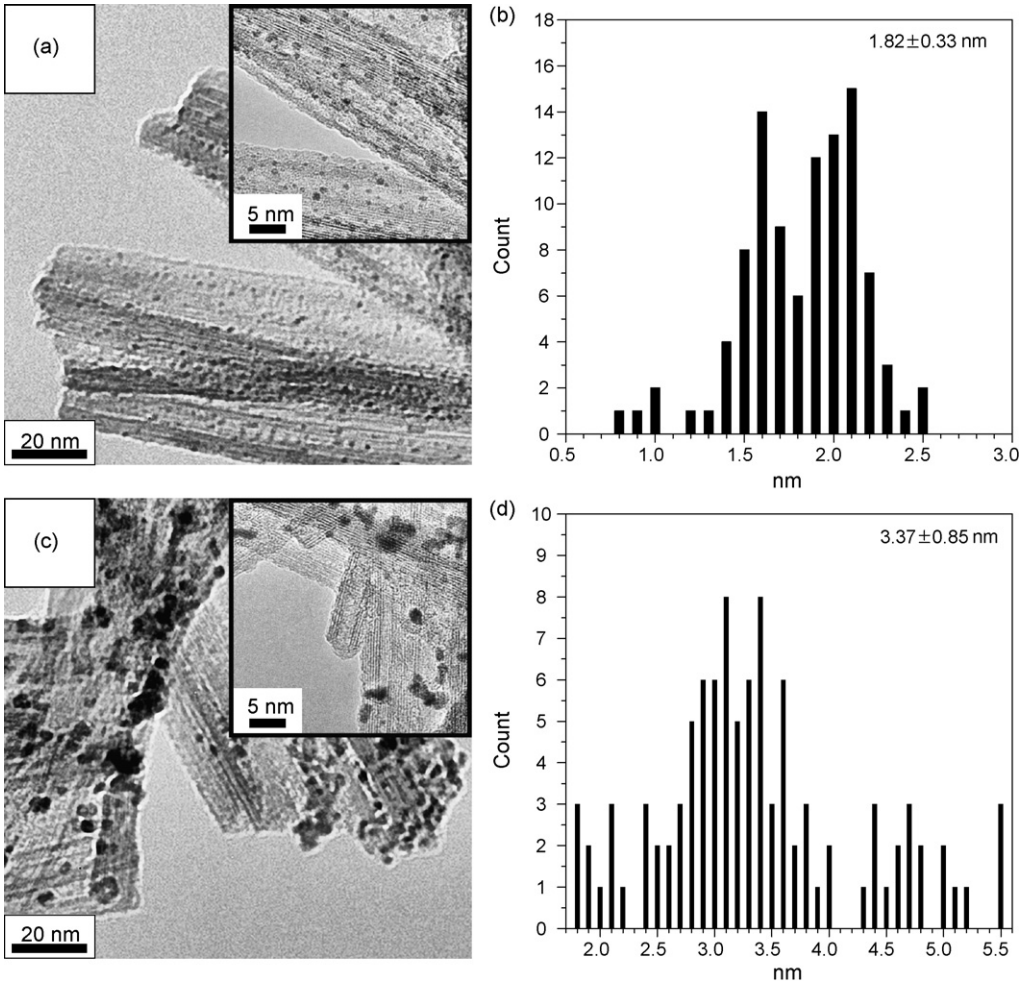

Fig. 12. Variation of gold particle size with the gold calcination temperature (a) TEM micrograph of AuNaTNT calcined at 473 K, (b) the gold particle size distribution in (a), (c) TEM micrograph of AuNaTNT calcined at 673 K, and (d) the particle size distribution in (c).

Table 2
Effect of calcination temperature on the oxidation states of Au and their distribution in AuNaTNT catalysts.

Calcination temperature of AuNaTNT (K)	BE and concentration of gold species			
	$Au^{\delta-}$ (mol%) [$4f_{7/2}$: 82.8 eV; $4f_{5/2}$: 86.5 eV]	Au^0 (mol%) [$4f_{7/2}$:83.8 eV; $4f_{5/2}$:87.5 eV]	Au^{+1} (mol%) [$4f_{7/2}$:86.0 eV; $4f_{5/2}$:89.7 eV]	Au^{+1}/Au^0
383	40.6	35.3	24.1	0.68
473	40.7	46.3	13.0	0.28
573	39.2	53.2	7.6	0.14
673	39.5	56.7	3.8	0.07

summarized in Fig. 13 and Table 2. The XPS showed that there were three Au species on the AuNaTNT surface, denoted as $Au^{\delta-}$, Au^0 and Au^{+1}. The gold species with a $4f_{7/2}$ binding energy of 82.8 eV, whose value is even lower than that of the metallic gold by 1 eV, was assigned to a gold species with a negative oxidation state, $Au^{\delta-}$ state. Such gold species had been reported before, and its formation was attributed to the transfer of the electron density from the support to the gold particle [10,52]. The concentration of $Au^{\delta-}$ species did not change with calcination temperature (and remained relatively constant at 40%), implying that the presence of this species was not the key point in the sub-ambient temperature oxidation of CO over AuNaTNT catalysts.

Although the binding energies for Au^{+1} (such as AuCl) and Au^{+3} (such as Au_2O_3) overlap [53], we had assigned the XPS peak with $4f_{7/2}$ binding energy of 86.0 eV to Au^{+1} because Au_2O_3 is known to be readily reduced even at room temperature (NaTNT seems to be very electron-rich, capable of donating electrons to gold particle and producing $Au^{\delta-}$ species). More interesting, as the calcination temperature of AuNaTNT increased, XPS results in Table 2 showed that the concentration of Au^{+1} species decreased and that of metallic gold (the peak with a $4f_{7/2}$ binding energy at 83.8 eV) increased simultaneously. This fact clearly demonstrated that Au^{+1} species are crucial in the sub-ambient CO oxidation reaction over AuNaTNT catalyst. The possible functions of Au^{+1} species are to provide Au–OH as part of the active site [54] and/or to stabilize the Au–CO bond through its positive oxidation charge (CO adsorbed more strongly on cationic gold than zerovalent gold [55]).

However, it should be pointed out that although AuNaTNT calcined at 673 K contained mostly reduced gold species ($Au^0 + Au^{\delta-} > 96\%$), the catalyst was still capable of achieving 100% CO conversion near room temperature (see Fig. 11).

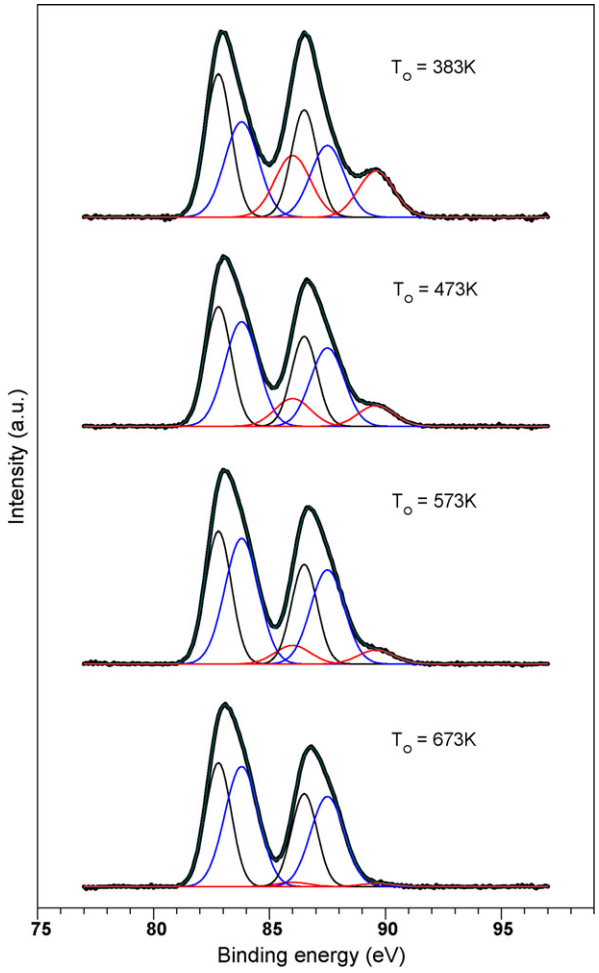

Fig. 13. Variation of XPS signals of gold with calcination temperature of gold particles (T_O). The Au loading used in this experiment was 2.2 wt.% and the NaTNT support was calcined at 673 K before ion exchange with gold.

4. Conclusions

Small gold particles with sizes of 1–2 nm could be prepared on the sodium trititanate nanotube surface by the ion exchange method. This titanate nanotube-supported gold catalyst could oxidize CO at sub-ambient temperatures, and the most active gold catalyst (Au383-S383-2.53) was able to achieve a $T_{50\%}$ of 218 K. The CO oxidation activity of AuNaTNT catalyst increased with gold loading (lower $T_{50\%}$). Increasing gold loading increased gold particle density on NaTNT without changing the gold particle size appreciably. Calcination of the NaTNT support lowered its surface area but did not affect its capability to accommodate gold particles. However, calcining NaTNT at higher than 383 K resulted in a activity loss, which was probably due to reduction of hydroxyl group and water content in AuNaTNT. The interaction between the gold particle and the NaTNT was probably strong, and calcining AuNaTNT at 673 K did not produce gold particles larger than 6 nm. XPS indicated there were three gold species, Au^0, Au^{+1} and $Au^{\delta-}$, in these AuNaTNT catalysts. Calcination of gold particles has no effect on the concentration of $Au^{\delta-}$ species, but higher calcination temperature will produce more Au^0 species at the consumption of Au^{+1} species. Lower concentration of Au^{+1} species in AuNaTNT, however, will decrease the catalytic activity of the AuNaTNT catalyst in the sub-ambient CO oxidation reaction.

Acknowledgements

C.-H. Lin is grateful for a grant from Nation Science Council of Taiwan (NSC-95-2113-M-018-007) to support this research. These authors also acknowledge Changhua Christian hospital for providing the medical accelerator for gold content analysis.

References

[1] M. Haruta, T. Kobayashi, H. Sano, N. Yamada, Chem. Lett. (1987) 405–408.
[2] M. Haruta, Catal. Today 36 (1997) 153–166.
[3] M. Haruta, N. Yamada, T. Kobayashi, S. Iijima, J. Catal. 115 (1989) 301–309.

[4] T. Sasaki, N. Koshizaki, M. Koinuma, Y. Matsumoto, Nanostruct. Mater. 12 (1999) 511–514.
[5] M. Okumura, S. Nakamura, S. Tsubota, T. Nakamura, M. Azuma, M. Haruta, Catal. Lett. 51 (1998) 53–58.
[6] J.M.C. Soares, P. Morrall, A. Crossley, P. Harris, M. Bowker, J. Catal. 219 (2003) 17–24.
[7] Y. Yuan, A.P. Kozlova, K. Asakura, H. Wan, K. Tsai, Y. Iwasawa, J. Catal. 170 (1997) 191–199.
[8] G.R. Bamwenda, S. Tsubota, T. Nakamura, M. Haruta, Catal. Lett. 44 (1997) 83–87.
[9] J.M.C. Soares, M. Bowker, Appl. Catal. A: Gen. 291 (2005) 136–144.
[10] S. Arrii, F. Morfin, A.J. Renouprez, J.L. Rousset, J. Am. Chem. Soc. 126 (2004) 1199–1205.
[11] J.-D. Grunwaldt, C. Kiener, C. Wögerbauer, A. Baiker, J. Catal. 181 (1999) 223–232.
[12] D. Guillemot, V. Yu Borovkov, V.B. Kazansky, M. Polisset-Thfoin, J. Fraissarda, J. Chem. Soc. Faraday Trans. 93 (1997) 3587–3591.
[13] B.K. Min, W.T. Wallace, D.W. Goodman, J. Phys. Chem. B 108 (2004) 14609–14615.
[14] N. Lopez, J.K. Nørskov, T.V.W. Janssens, A. Carlsson, A. Puig-Molina, B.S. Clausen, J.-D. Grunwaldt, J. Catal. 225 (2004) 86–94.
[15] B.K. Min, W.T. Wallace, A.K. Santra, D.W. Goodman, J. Phys. Chem. B 108 (2004) 16339–16343.
[16] C.K. Costello, M.C. Kung, H.-S. Oh, Y. Wang, H.H. Kung, Appl. Catal. A: Gen. 232 (2002) 159–168.
[17] J.L. Margitfalvi, M. Hegedüs, Á. Szegedi, I. Sajó, Appl. Catal. A: Gen. 272 (2004) 87–97.
[18] K. Qian, Z. Jiang, W. Huang, J. Mol. Catal. A: Chem. 264 (2007) 26–32.
[19] A.K. Tripathi, V.S. Kamble, N.M. Gupta, J. Catal. 187 (1999) 332–342.
[20] U.R. Pillai, S. Deevi, Appl. Catal. A: Gen. 299 (2006) 266–273.
[21] W.-C. Li, M. Comotti, F. Schüth, J. Catal. 237 (2006) 190–196.
[22] M.M. Schubert, S. Hackenberg, A.C. van Veen, M. Muhler, V. Plzak, R.J. Behm, J. Catal. 197 (2001) 113–122.
[23] M. Haruta, Cattech 6 (2002) 102–115.
[24] T. Kasuga, M. Hiramatsu, A. Hoson, T. Sekino, K. Niihara, Langmuir 14 (1998) 3160–3163.
[25] T. Kasuga, M. Hiramatsu, A. Hoson, T. Sekino, K. Niihara, Adv. Mater. 11 (1999) 1307–1311.
[26] M. Zhang, Z. Jin, J. Zhang, X. Guo, J. Yang, W. Li, X. Wang, Z. Zhang, J. Mol. Catal. A: Chem. 217 (2004) 203–210.
[27] S. Zhang, Q. Chen, L.M. Peng, Phys. Rev. B 71 (2005), 014104-1–014104-11.
[28] A. Nakahira, W. Kato, M. Tamai, T. Isshiki, K. Nishio, J. Mater. Sci. 39 (2004) 4239–4245.
[29] R. Ma, Y. Bando, T. Sasaki, Chem. Phys. Lett. 380 (2003) 577–582.
[30] H. Irawa, S. Klkkawa, M. Koirunj, J. Phys. Chem. 86 (1982) 5023–5026.
[31] I.M. El-Naggar, E.S. Zakaria, I.M. Ali, Sep. Sci. Technol. 39 (2004) 959–974.
[32] S. Mendioroz, A.B. Martín-Rojo, F. Rivera, J.C. Martín, A. Bahamonde, M. Yates, Appl. Catal. B: Environ. 64 (2006) 161–170.
[33] D.V. Bavykin, A.A. Lapkin, P.K. Plucinski, J.M. Friedrich, F.C. Walsh, J. Catal. 235 (2005) 10–17.
[34] X. Sun, Y. Li, Chem. Eur. J. 9 (2003) 2229–2238.
[35] R. Zanella, C. Louis, Catal. Today 107–108 (2005) 768–777.
[36] Q. Chen, G.H. Du, S. Zhang, L.-M. Peng, Acta Cryst. 58 (2002) 587–593.
[37] F. Moreau, G.C. Bond, A.O. Taylor, J. Catal. 231 (2005) 105–114.
[38] N. Lopez, T.V.W. Janssens, B.S. Clausen, Y. Xu, M. Mavrikakis, T. Bligaard, J.K. Nørskov, J. Catal. 223 (2004) 232–235.
[39] I.N. Remediakis, N. Lopez, J.K. Nørskov, Appl. Catal. A: Gen. 291 (2005) 13–20.
[40] M. Mavrikakis, P. Stoltze, J.K. Nørskov, Catal. Lett. 64 (2000) 101–106.
[41] H. Tsai, E. Hu, K. Perng, M. Chen, J.-C. Wu, Y.-S. Chang, Surf. Sci. Lett. 537 (2003) L447–L450.
[42] W. Ke, Z. Min, J. Zhensheng, Z. Shunli, Y. Jianjun, Z. Zhijun, Chin. J. Catal. 26 (2005) 283–286.
[43] Z. Yan, S. Chinta, A.A. Mohamed, J.P. Fackler Jr., D.W. Goodman, J. Am. Chem. Soc. 127 (2005) 1604–1605.
[44] A. Sanchez, S. Abbet, U. Heiz, W.-D. Schneider, H. Häkkinen, R.N. Barnett, U. Landman, J. Phys. Chem. A 103 (1999) 9573–9578.
[45] M. Daté, M. Okumura, S. Tsubota, M. Haruta, Angew. Chem. Int. Ed. 43 (2004) 2129–2132.
[46] C.K. Costello, J.H. Yang, H.Y. Law, Y. Wang, J.-N. Lin, L.D. Marks, M.C. Kung, H.H. Kung, Appl. Catal. A: Gen. 243 (2003) 15–24.
[47] M. Daté, M. Haruta, J. Catal. 201 (2001) 221–224.
[48] L.M. Liu, B. McAllister, H.Q. Ye, P. Hu, J. Am. Chem. Soc. 128 (2006) 4017–4022.
[49] J.G. Wang, B. Hammer, Phys. Rev. Lett. 97 (2006), 136107-1–136107-4.
[50] M. Daté, Y. Ichihashi, T. Yamashita, A. Chiorino, F. Boccuzzi, M. Haruta, Catal. Today 72 (2002) 89–94.
[51] E.D. Park, J.S. Lee, J. Catal. 186 (1999) 1–11.
[52] A.-Q. Wang, J.-H. Liu, S.D. Lin, T.-S. Lin, C.-Y. Mou, J. Catal. 233 (2005) 186–197.
[53] A.M. Visco, F. Neri, G. Neri, A. Donato, C. Milone, S. Galvagno, Phys. Chem. Chem. Phys. 1 (1999) 2869–2873.
[54] H.H. Kung, M.C. Kung, C.K. Costello, J. Catal. 216 (2003) 425–432.
[55] J.C. Fierro-Gonzalez, B.C. Gates, Catal. Today 122 (2007) 201–210.